Measuring Bipartite Spin Correlations of Lattice-Trapped Dipolar Atoms

Youssef Aziz Alaoui, 1,2,* Sean R. Muleady, 3,4,5,6,* Edwin Chaparro, 3,4 Youssef Trifa, 7 Ana Maria Rey, 3,4

Tommaso Roscilde, Bruno Laburthe-Tolra, 2,1 and Laurent Vernac, 1,2

1 Université Sorbonne Paris Nord, Laboratoire de Physique des Lasers, F-93430 Villetaneuse, France

2 CNRS, UMR 7538, LPL, F-93430, Villetaneuse, France

3 JILA, NIST and Department of Physics, University of Colorado, Boulder, USA

4 Center for Theory of Quantum Matter, University of Colorado, Boulder, Colorado 80309, USA

5 Joint Center for Quantum Information and Computer Science, NIST and University of Maryland, College Park, Maryland 20742, USA

6 Joint Quantum Institute, NIST and University of Maryland, College Park, Maryland 20742, USA

7 Univ Lyon, Ens de Lyon, CNRS, Laboratoire de Physique, F-69342 Lyon, France

(Received 16 April 2024; revised 13 September 2024; accepted 11 October 2024; published 13 November 2024)

We demonstrate a bipartition technique using a superlattice architecture to access correlations between alternating planes of a mesoscopic array of spin-3 chromium atoms trapped in a 3D optical lattice. Using this method, we observe that out-of-equilibrium dynamics driven by long-range dipolar interactions lead to spin anticorrelations between the two spatially separated subsystems. Our bipartite measurements reveal a subtle interplay between the anisotropy of the 3D dipolar interactions and that of the lattice structure, without requiring single-site addressing. We compare our results to theoretical predictions based on a truncated cumulant expansion and a new cluster semiclassical method that we use to investigate correlations at the microscopic scale. Comparison with a high-temperature analytical model reveals quantum thermalization at a high negative spin temperature.

DOI: 10.1103/PhysRevLett.133.203401

Introduction—The study of fluctuations between subensembles of a quantum system is crucial to reveal some of the most fundamental concepts of quantum mechanics such as entanglement [1], Einstein-Podolsky-Rosen (EPR) steering [2], Bell correlations [3], quantum scrambling [4,5], and quantum thermalization [6–8]. When individual addressing of each particle is available, advanced techniques have allowed investigation of entanglement entropy [9–11], purity certification [12], quantum thermalization [12–14], quantum scrambling [15], and out-of-time-order correlators [16,17]. For mesoscopic systems, where quantum tomography is impractical, demonstration of EPR correlations was obtained by measuring the relative fluctuations between two subsystems of a bulk BEC [18–21].

Platforms harnessing dipolar interacting particles are of particular interest for studying the propagation of quantum correlations [22–29], which can be very different compared to those induced by finite-range interactions, due to the high group velocity of elementary excitations [30–32]. In these platforms, the 3D anisotropy plays an unavoidable role [33,34]. Experimentally, individual addressing in dipolar systems is mostly available for particles with strong electric dipole moment, such as in Rydberg atoms [35], heteronuclear molecules in optical lattices [14,36], or in tweezer arrays [37–39]. In the case of magnetic atoms [40], the use of short-period lattices, necessary to boost the

strength of the interactions, makes individual addressing challenging [see, however, a recent realization in two-dimensions (2D)] [41]). Besides, individual addressing remains extremely difficult in 3D [42]. It is thus relevant to develop new tools based on collective measurements of subsystems in order to study correlations in dipolar 3D systems.

Here we implement bipartition within a 3D optical lattice loaded with strongly magnetic chromium atoms, quenched into an out-of-equilibrium spin state. We use a superlattice in order to separate alternating lattice planes and thus perform bipartite measurements that ensure a large interface between both subsystems. We measure the growth of anisotropic spin correlations at the level of the standard quantum projection noise, revealing anticorrelations between the collective magnetization of the subsystems. We compare our results to different advanced numerical methods. In particular, we introduce a refinement of the generalized discrete truncated Wigner semiclassical approximation (GDTWA) [43]), in which certain local correlations are treated exactly. Furthermore, we perform calculations for the thermalized state that is expected at long time [33], using a high-temperature expansion. Our combined experimental and theoretical analysis demonstrates that bipartite correlations are inherently sensitive to the anisotropy of the system and to the value and sign of the effective spin temperature at equilibrium.

Description of the spin system and bipartition protocol— The N spin s=3 chromium atoms are pinned at the

^{*}These two authors contributed equally to this work.

antinodes of a 3D lattice. An external 0.75 gauss magnetic field ${\bf B}$, which is strong enough to generate Zeeman splittings much larger than nearest-neighbor dipolar interactions, ensures that only processes that conserve the total magnetization are energetically allowed. The dynamics are thus described by the following effective xxz (${\bf B}\|{\bf z}$) Hamiltonian, together with a one-body term:

$$\hat{H} = \sum_{i>j}^{N} V_{i,j} \left[\hat{s}_{z,i} \hat{s}_{z,j} - \frac{1}{2} (\hat{s}_{x,i} \hat{s}_{x,j} + \hat{s}_{y,i} \hat{s}_{y,j}) \right] + B_{Q} \sum_{i}^{N} \hat{s}_{z,i}^{2}$$

$$(1)$$

with $V_{i,j} = V_{dd}(1 - 3\cos^2\theta_{i,j})/r_{i,j}^3, \ V_{dd} = \mu_0(g_L\mu_B)^2/4\pi,$ where μ_0 is the magnetic permeability of vacuum, $g_L \simeq 2$ the Landé factor, and μ_B the Bohr magneton. $r_{i,j}$ is the distance between atoms, and $\theta_{i,j}$ the angle between their interatomic axis and **B**. $\hat{\mathbf{s}}_i = (\hat{s}_{x,i}, \hat{s}_{y,i}, \hat{s}_{z,i})$ are spin-3 angular momentum operators for atom i when a site is populated by a single atom. $B_{\rm O}$ describes the strength of a quadratic Zeeman term that accounts for tensor light shifts proportional to the trapping laser intensity [33]. For our experimental parameters, B_0 can be determined only at the kHz level from available spectroscopic data and is therefore considered as a free parameter in this Letter. The 3D lattice, created by five 532 nm laser beams, is anisotropic [44] and corresponds to a one-dimensional (1D) array of relatively well separated planes, each containing a two-dimensional (2D) lattice (XZ planes in Fig. 1). The quantization axis z, set by **B**, is nearly parallel to these planes and perpendicular to the spatial Z axis.

From an initial noncorrelated spin state, pairwise entanglement due to dipolar interactions is expected to grow most rapidly at short range. To best reveal this growth of quantum correlations we overlap the native lattice structure with a superlattice, creating an array of double wells [51,52] that define two interleaved subensembles, which we refer to as A and B. Compared to a bipartition defined by two spatially separated ensembles meeting at a single plane [18–20], our bipartition guarantees each atom in the A sublattice possesses nearest neighbors in the B sublattice. This enhances the intersublattice connectivity by a factor of $\sim N^{1/D}$, where D=3 is the dimensionality, thus improving our signal-to-noise ratio for the correlation measurements. We note that longer-range correlators could be measured by increasing the frequency mismatch between the lasers of the bichromatic 1D lattice (see Ref. [53]).

The bipartition scheme is detailed in Fig. 1. After dynamically evolving the system in the 3D lattice, we adiabatically superimpose a 1064 nm retro-reflected beam overlapped with one retro-reflected 532 nm beam (H1 beam) [44]. We then adiabatically switch off all lattice beams at 532 nm except for H1, creating a bichromatic 1D lattice. Finally, we switch off H1 abruptly, letting atoms evolve in the 1064 nm 1D lattice for approximately one-

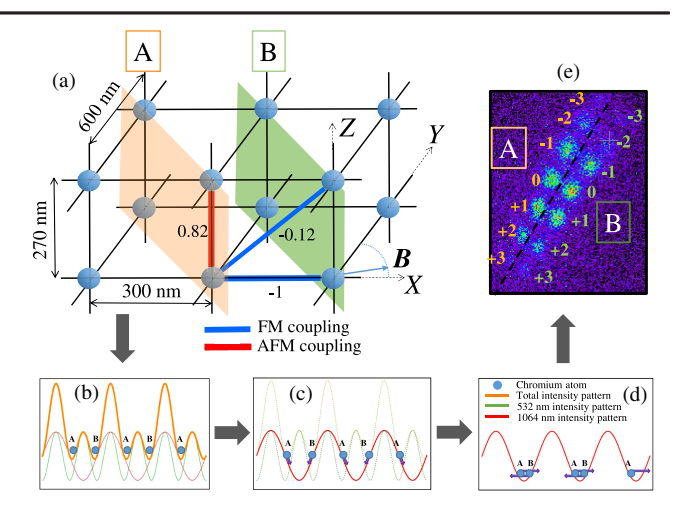


FIG. 1. Sketch of the experiment. The spin dynamics takes place in a 3D anisotropic lattice, with a combination of ferromagnetic (FM) and anti-ferromagnetic (AFM) dipolar couplings in the XZ plane. The strongest couplings (in arbitrary units) are indicated in (a). The addition of an infrared (IR) laser at the end of the dynamics creates a double-well structure that gives rise to two spin subsystems A and B (b). Atoms then evolve in the pure 1D lattice created by the IR laser for a quarter period (c),(d), which allows for spatial separation of the two subsystems after time of flight, as a result of opposite momenta conveyed to the atoms (d). Stern-Gerlach separation yields measurement of the magnetization of both subsystems with fluorescence imaging. (e) Image of the seven spin states at t=15 ms for both subsystems.

fourth of the oscillation time within one lattice site. This effectively implements a $\pi/2$ rotation in phase space, translating the opposing positions of the atoms into opposite momenta [54]. A time of flight of 14 ms then separates the atoms in two subsystems that correspond to the original A and B subsystems. Stern-Gerlach separation during time of flight allows measurement of the seven spin components within each subsystem, for which we use fluorescence imaging onto an electron multiplying CCD camera.

Collective fluctuations and pairwise correlators—In this Letter we measure the following two-point correlators associated with the magnetization

$$C_z^{\sigma,\sigma'} = \sum_{i \in \sigma, j \in \sigma', i \neq j} \left(\langle \hat{s}_{z,i} \hat{s}_{z,j} \rangle - \langle \hat{s}_{z,i} \rangle \langle \hat{s}_{z,j} \rangle \right). \tag{2}$$

From this, we define the correlator for the whole sample, which we denote C_z for simplicity $(\sigma = \sigma' = A \cup B)$; the subsystems correlators, C_z^A or C_z^B $(\sigma = \sigma' = A \text{ or } B)$; and the intersystem correlator, C_z^{AB} $(\sigma = A, \sigma' = B)$. Defining subsystem spin operators $\hat{S}_z^{\sigma} = \sum_{i \in \sigma} \hat{s}_{z,i}$, we note that $C_z^{AB} = \text{Cov}(\hat{S}_z^A, \hat{S}_z^B)$.

 C_z, C_z^A, C_z^B are related to fluctuations of the spin component \hat{S}_z^{σ} [55]: $C_z^{\sigma} = \operatorname{Var}(\hat{S}_z^{\sigma}) - \Sigma_z^{\sigma}$, with $\operatorname{Var}(\hat{S}_z^{\sigma})$ the variance of \hat{S}_z^{σ} , and $\Sigma_z^{\sigma} = \sum_{i \in \sigma} \langle \hat{S}_{z,i}^2 \rangle - \langle \hat{S}_{z,i} \rangle^2$. As we can

neglect inhomogeneities in our system [56], we assume $\langle \hat{s}_{z,i} \rangle = 0$ for all i. From the measurement of spin populations $P^{\sigma}_{m_s}$ ($-3 \le m_s \le 3$), we then have $\langle \hat{S}^{\sigma}_z \rangle = \sum_{m_s \in \sigma} m_s P^{\sigma}_{m_s}$ and $\Sigma^{\sigma}_z = \sum_{m_s \in \sigma} m_s^2 P^{\sigma}_{m_s}$ [56]. As the collective spin $\hat{S}_z = \hat{S}^A_z + \hat{S}^B_z$ commutes with the

As the collective spin $\hat{S}_z = \hat{S}_z^A + \hat{S}_z^B$ commutes with the Hamiltonian Eq. (1), $Var(\hat{S}_z)$ is expected to remain equal to its initial value (3N/2 in our case, see below); on the other hand, variances of the subsystem magnetizations are free to vary from their initial values ($3N_{A,B}/2$, for $N_{A,B}$ the total number of particles in each subsystem) as correlations develop between the two subsystems:

$$\operatorname{Var}(\hat{S}_z) = \operatorname{Var}(\hat{S}_z^A) + \operatorname{Var}(\hat{S}_z^B) + 2C_z^{AB}. \tag{3}$$

Therefore, our bipartition scheme allows probing of correlations in each subsystem, assuming homogeneity, as well as correlations between the subsystems quantified by the covariance featured in the right part of Eq. (3), *without* assuming homogeneity.

Experimental results—Initially, the lattice contains an average of 1.5×10^4 spin-3 atoms, polarized in the minimal Zeeman energy state $m_s = -3$. A deep Mott insulator state regime is reached, excluding particle transport during the duration of dynamics. To initialize dynamics, atoms are quenched to an excited state via a radio frequency $\pi/2$ pulse. This prepares a coherent spin state with all spins pointing orthogonal to **B**. The out-of-equilibrium spin dynamics leads to an evolution of the seven spin populations P_{m_s} measured in the basis of the quantization axis. From measurement of these spin populations, we obtain Σ_z^{σ} and $\operatorname{Var}(\hat{S}_z^{\sigma})$ (see above) and infer C_z , C_z^A , C_z^B . The intersystem correlators C_z^{AB} are obtained from the relation $C_z = C_z^A + C_z^B + 2C_z^{AB}$.

For measuring the variances $Var(\hat{S}_z^{\sigma})$, eight series of 70 images were recorded in order to reduce finite sampling noise. In addition, we have performed an exhaustive data analysis by carefully characterizing each fundamental and technical noise source in our detection scheme, using the law of total (co)variances. We have also employed the Delta method [57] to account for corrections to our variance measurements arising from fluctuations in both the total and subensemble atom numbers (see Ref. [58]).

Results for correlators for three durations of spin dynamics are shown in Fig. 2. Data at t=0 ms provide a benchmark; the global correlations have nearly equilibrated at t=30 ms [33]. Note that the atom number is time dependent due to dipolar relaxation losses at short times. These concern the doubly occupied sites, which exist mostly at the center of the typical wedding-cake distribution [59] obtained in the Mott regime: atoms in these sites are lost typically after 10 ms. These losses have been shown not to substantially affect the spin properties of the shell with unit filling that survives [56]. We find that negative correlations $C_z < 0$ develop within the whole sample

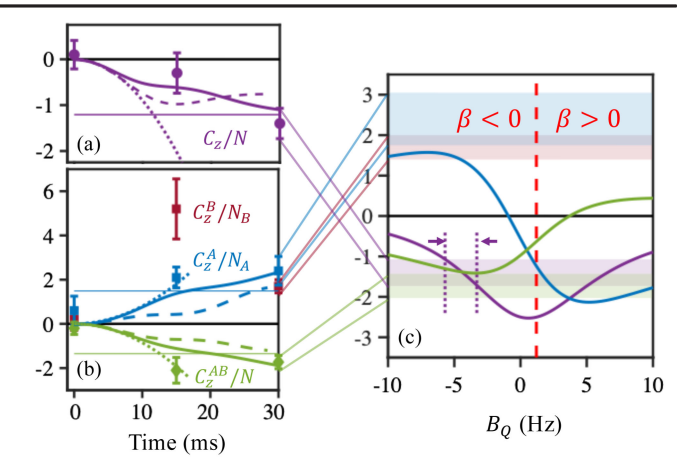


FIG. 2. Experimental results and model comparisons for correlators. Dynamics of collective (a) and subsystems (b) correlators. For experimental data, full error bars correspond ± 1 statistical standard error. We show theoretical results obtained via a short time expansion (dotted), truncated cumulant calculations (dashed), and cluster-GDTWA simulations (solid). Steady state expectations from a high-temperature expansion are denoted as thin horizontal lines. (c) Correlators in the thermalized state as a function of the quadratic term B_Q . Solid lines denote the values of $C_{z,\rm th}/N$ (purple), $C_{z,\rm th}^A/N_A$ (blue), and $C_{z,\rm th}^{AB}/N$ (green). The shaded regions show the corresponding confidence intervals for experimental data at 30 ms, including the confidence interval for C_z^B/N_B (red shaded region). The dashed red line indicates B_O for which an infinite temperature $\beta = 0$ is predicted, with $\beta < 0$ $(\beta > 0)$ to the left (right) of this line. The region bounded by the purple dot-dashed lines denotes the range of $B_O < 0$ compatible with the measured C_z/N error bars at 30 ms.

[Fig. 2(a)] and recover prior results obtained *without* implementing bipartition [56]: this shows that our bipartition process does not suffer from systematic effects that could arise, e.g., from collisions. In contrast, we find that positive correlations build up within the subsystems, while the two subsystems become anticorrelated [Fig. 2(b)]. This measurement of the anisotropy of correlators via bipartition constitutes the main result of this Letter. We now discuss how this arises.

Thermalization to a negative spin temperature—In order to gain physical insight, we first discuss results of our calculations for the state that is expected at long time for our system, assuming it to be chaotic and undergo quantum thermalization [33]. We characterize this state by a thermal-like density matrix, which should in principle account for all conserved quantities. While all powers of \hat{H} and \hat{S}_z are conserved in the dynamics, we only require the thermal state to reproduce the average energy and variance of \hat{S}_z . These constitute all the conserved quantities which are quadratic in the spin moments and which thus most directly influence the two-point correlations of interest. Moreover the variance of \hat{S}_z completely determines the \hat{S}_z distribution in the initial state, since the fluctuations of \hat{S}_z are Gaussian.

Hence, we take $\hat{\rho}_{\rm th} \propto \exp(-\beta \hat{H} - \mu_2 \hat{S}_z^2)$, where β is the inverse temperature and μ_2 a Lagrange multiplier. We have implicitly also included a term $\mu_1 \hat{S}_z$ with $\mu_1 = 0$, which fixes $\langle \hat{S}_z \rangle = 0$.

In the case of a high thermalization temperature, which we expect for our system and initial conditions, we can expand $\hat{\rho}_{th}$ to first order; corresponding expressions for β and μ_2 are given in [44]. Assuming $N_A = N_B = N/2$, we obtain the following expression for thermal correlators:

$$C_{z,\text{th}}^{\sigma} = -32N(\beta \overline{V_{\sigma}} + \mu_2 N/4). \tag{4}$$

Subsystems correlators are given by $\overline{V_A} = \overline{V_B} = \sum_{i_A \neq j_A} V_{i_A,j_A}/2N$, and the intersystem correlator is given by $\overline{V_{AB}} = \sum_{i_A,j_B} V_{i_A,j_B}/2N$. Equation (4) shows that $C_{z,\text{th}}^A = C_{z,\text{th}}^B = C_{z,\text{th}}/4$ if $\overline{V_A} = \overline{V_{AB}}$. On the other hand, any difference between $C_{z,th}^A = C_{z,th}^B$ and $C_{z,th}^{AB}$ reveals anisotropy, as in our case. We numerically evaluate $\overline{V_A}$ and $\overline{V_{AB}}$, which depend on both lattice structure and size [44] and infer thermal correlators for a given B_Q , as shown in Fig. 2(c). Our measurements, which indicate that C_z^A and C_z^B (C_z^{AB}) evolve toward a positive (negative) value, exclude thermalization at positive temperature as well as a positive sign of B_O with a high confidence margin, as shown in Fig. 2(c). By contrast, these conclusions cannot be reached when measuring C_z only, as the value of C_z is compatible with both a positive and a negative B_Q : bipartition enables us to pinpoint the up-to-now elusive sign of B_O . This demonstrates the utility of bipartite measurements for capturing fundamental features of quantum thermalization. In turn, having identified thermalization at negative temperature yields a physical explanation for the development of negative interspecies correlations in the thermal state, despite the predominantly ferromagnetic couplings between the A and B subsystems (see Fig. 1): for thermalization at a positive temperature, such couplings would lead to positive correlations.

Our results thus imply that the spin degrees of freedom thermalize to a negative temperature $T \approx -2.5$ nK, whose absolute value is high enough that our thermal expansion for $\hat{\rho}_{th}$ is valid [33]. Such a negative temperature is possible when the energy spectrum is bounded by above [60] and has been observed in cold atom experiments for the external degrees of freedom [61] and for the spin degrees of freedom [62] in an *open* Fermi-Hubbard gas. We stress the versatility of our system: thermalization can be tuned to large positive temperature by controlling the sign of B_Q (see the expression for β in [44]), while changing the orientation of B along D would invert the antiferromagnetic-ferromagnetic character of the intersublattice couplings; see Fig. 1(a).

Numerical methods—We now turn to our numerical models. Exact second-order short-time expansions (see

Ref. [44]) show that no simple relationship exists between short-time and long-time behaviors, as we will discuss below for the microscopic correlations. For intermediate times, we have developed numerical simulations based on truncated cumulant expansion (TCE), in which order $n \ge 3$ cumulants of quantum fluctuations are set to zero (see Ref. [44]); and on the GDTWA [43,63], which has been successfully used in comparison with magnetic-atom experiments in the recent past [33,34,56]. We have found that GDTWA appears to overestimate the expected thermalization value for subsystems correlators (see also [64]). We have therefore studied a cluster-GDTWA approach [43,65], in which neighboring pairs of spins are clustered together, so that their quantum correlations are treated exactly, while the correlations between clusters are treated semiclassically. Cluster GDTWA leads to a marked improvement over standard GDTWA in capturing the long-time thermal predictions [44], even though we have limited our calculations here to pairs of spin-3 particles owing to the exponential complexity scaling in cluster size.

At short times all three theoretical predictions for the dynamics coincide; see Fig. 2(a). After about 7 ms, differences begin to arise between cluster GDTWA and TCE, which we interpret as the onset of cumulants with order 3 and higher in the quantum spin fluctuations. We point out that none of our models include the dipolar losses that affect the doubly-occupied sites at short times: these losses do not alter the agreement with measured bipartite correlations.

Microscopic structure of the correlations—We finally discuss the dynamics of correlations at the microscopic scale, as revealed by our theoretical approaches. In Fig. 3, we show our results for the correlation maps in the XZplane, containing the strongest couplings in our 3D anisotropic lattice; even-odd columns in Fig. 3 correspond to subsystems A and B in Fig. 1. We compare the cluster-GDTWA calculations and short time expansions for the correlators [Figs. 3(a) and 3(b)] to their thermal values given in Fig. 3(c). We find that the next-nearest-neighbor correlations initially grow more rapidly than the nearestneighbor correlations despite smaller couplings $V_{i,j}$. This can be explained by our second-order short time expansion; see Ref. [44]. Moreover, nearest-neighbor correlations change in sign along the time evolution [Fig. 3(a)]. We find that this peculiar behavior is a consequence of the negative sign of B_Q . Indeed, for nearest neighbors, the short time expansion is dominated by $\langle \hat{s}_z^i \hat{s}_z^j \rangle \propto t^2 B_O V_{i,j}$ so that the sign of the correlator and of the coupling are opposite for $B_Q < 0$. In the thermal state, the correlation map is instead identical to the interactions map [Figs. 3(c) and 3(d)] up to a global shift [44]. Our microscopic analysis thus demonstrates that the sign inversion of correlators at short distance is deeply linked to thermalization at high negative temperature, dictated by the negative value of B_O . Interestingly, the sign of the subsystem correlator C_z^{AB}

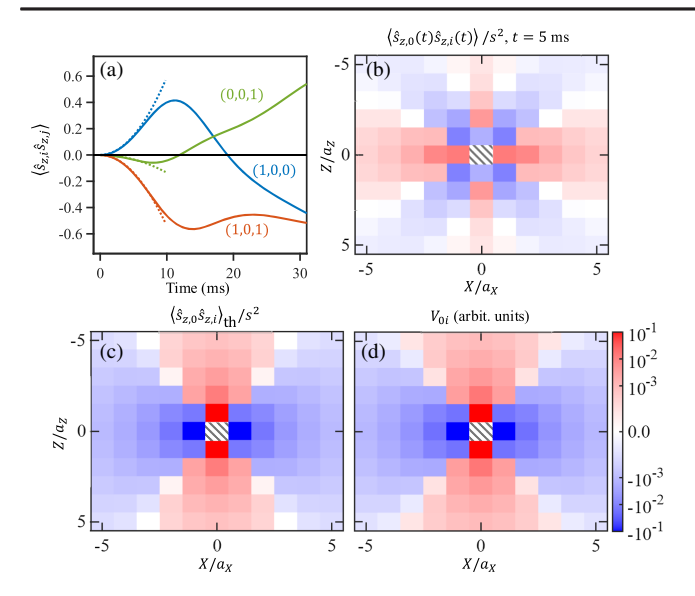


FIG. 3. Correlations at the microscopic level. In a given XZ plane, the bipartition separates odd and even sites along the X axis. (a) Dynamics of the $\langle \hat{s}_{z,i} \hat{s}_{z,j} \rangle$ correlators corresponding to sites i and j separated by one lattice site along the X dimension (blue), Z dimension (green), or both (orange), computed via cluster GDTWA (full), or short-time expansions (dotted). (b) Offsite correlations at t=5 ms computed via a short-time expansion; the X/Z distances between the origin and lattice sites i are normalized by the corresponding lattice spacing a_X/a_Z . Values of corresponding (c) thermal correlators and (d) interaction matrix elements.

remains negative throughout the evolution. At short times C_z^{AB} is dominated by the negative value of the correlations at separation (X,Y,Z)=(1,0,1); at longer times the correlations at separation (1,0,0) turn negative and further contribute to the negative value of C_z^{AB} .

Conclusion—We have experimentally implemented a bipartition of magnetic atoms in a 3D optical lattice prepared in a Mott insulator state and have used this scheme to track short-range spin correlations. The observed structure of correlations reveals the anisotropic nature of our dipolar spin system. Extending our analysis to correlations along orthogonal spin components would enable entanglement certification [66].

Comparing our results to various numerical methods led to several additional insights. The predictions of a thermal ensemble, when matched to our late-time experimental results, allowed us to unambiguously fix the Hamiltonian parameters and to conclude that thermalization takes place at a high, negative temperature. The observed evolution of the correlation map is highly nontrivial, with correlations changing sign between the short-time evolution and the long-time one. Our Letter demonstrates that magnetic-atom quantum simulators can act as an efficient test bed for state-of-the-art models of out-of-equilibrium quantum dynamics and exhibit peculiar quantum thermalization, due to the power-law and anisotropic nature of dipolar interactions [67,68].

Acknowledgments—We acknowledge careful review of this manuscript and useful comments from Joanna W. Lis and Sanaa Agarwal. The Villetaneuse and Lyon groups acknowledge financial support from CNRS. The Villetaneuse group acknowledges financial support from Agence Nationale de la Recherche (project No. EELS ANR-18-CE47-0004), QuantERA ERA-NET (MAQS project). S. R. M. is supported by the NSF QLCI Grant No. OMA-2120757. A. M. R. is supported by AFOSR MURI FA9550-21-1-0069, the ARO single investigator Award No. W911NF24-1-0128, the NSF JILA-PFC PHY-2317149 grants, and by NIST.

- R. Horodecki, P. Horodecki, M. Horodecki, and K. Horodecki, Rev. Mod. Phys. 81, 865 (2009).
- [2] D. Cavalcanti and P. Skrzypczyk, Rep. Prog. Phys. 80, 024001 (2016).
- [3] N. Brunner, D. Cavalcanti, S. Pironio, V. Scarani, and S. Wehner, Rev. Mod. Phys. 86, 419 (2014).
- [4] P. Hosur, X.-L. Qi, D. A. Roberts, and B. Yoshida, J. High Energy Phys. 02 (2016) 004.
- [5] G. Styliaris, N. Anand, and P. Zanardi, Phys. Rev. Lett. 126, 030601 (2021).
- [6] D. Poilblanc, Phys. Rev. B 84, 045120 (2011).
- [7] A. P. Luca D'Alessio, Yariv Kafri, and M. Rigol, Adv. Phys. 65, 239 (2016).
- [8] T. Mori, T. N. Ikeda, E. Kaminishi, and M. Ueda, J. Phys. B 51, 112001 (2018).
- [9] R. Islam, R. Ma, P. M. Preiss, M. Eric Tai, A. Lukin, M. Rispoli, and M. Greiner, Nature (London) 528, 77 (2015).
- [10] T. Brydges, A. Elben, P. Jurcevic, B. Vermersch, C. Maier, B. P. Lanyon, P. Zoller, R. Blatt, and C. F. Roos, Science 364, 260 (2019).
- [11] M. Niknam, L. F. Santos, and D. G. Cory, Phys. Rev. Lett. 127, 080401 (2021).
- [12] A. M. Kaufman, M. E. Tai, A. Lukin, M. Rispoli, R. Schittko, P. M. Preiss, and M. Greiner, Science 353, 794 (2016).
- [13] C. Neill et al., Nat. Phys. 12, 1037 (2016).
- [14] L. Christakis, J. S. Rosenberg, R. Raj, S. Chi, A. Morningstar, D. A. Huse, Z. Z. Yan, and W. S. Bakr, Nature (London) **614**, 64 (2023).
- [15] M. S. Blok, V. V. Ramasesh, T. Schuster, K. O'Brien, J. M. Kreikebaum, D. Dahlen, A. Morvan, B. Yoshida, N. Y. Yao, and I. Siddiqi, Phys. Rev. X 11, 021010 (2021).
- [16] J. Li, R. Fan, H. Wang, B. Ye, B. Zeng, H. Zhai, X. Peng, and J. Du, Phys. Rev. X 7, 031011 (2017).
- [17] M. Gärttner, J. G. Bohnet, A. Safavi-Naini, M. L. Wall, J. J. Bollinger, and A. M. Rey, Nat. Phys. 13, 781 (2017).
- [18] K. Lange, J. Peise, B. Lücke, I. Kruse, G. Vitagliano, I. Apellaniz, M. Kleinmann, G. Tóth, and C. Klempt, Science **360**, 416 (2018).
- [19] M. Fadel, T. Zibold, B. Décamps, and P. Treutlein, Science 360, 409 (2018).
- [20] P. Kunkel, M. Prüfer, H. Strobel, D. Linnemann, A. Frölian, T. Gasenzer, M. Gärttner, and M. K. Oberthaler, Science 360, 413 (2018).

- [21] P. Colciaghi, Y. Li, P. Treutlein, and T. Zibold, Phys. Rev. X 13, 021031 (2023).
- [22] T. Kuwahara and K. Saito, Phys. Rev. Lett. 126, 030604 (2021).
- [23] A. Lerose and S. Pappalardi, Phys. Rev. Res. 2, 012041(R) (2020).
- [24] J. Eisert, M. van den Worm, S. R. Manmana, and M. Kastner, Phys. Rev. Lett. 111, 260401 (2013).
- [25] M. A. Perlin, C. Qu, and A. M. Rey, Phys. Rev. Lett. 125, 223401 (2020).
- [26] T. Comparin, F. Mezzacapo, and T. Roscilde, Phys. Rev. Lett. 129, 150503 (2022).
- [27] T. Roscilde, T. Comparin, and F. Mezzacapo, Phys. Rev. Lett. 131, 160403 (2023).
- [28] Y. Trifa and T. Roscilde, arXiv:2309.05368.
- [29] Z.-X. Gong, M. Foss-Feig, F. G. S. L. Brandão, and A. V. Gorshkov, Phys. Rev. Lett. 119, 050501 (2017).
- [30] I. Frérot, P. Naldesi, and T. Roscilde, Phys. Rev. Lett. 120, 050401 (2018).
- [31] L. Cevolani, J. Despres, G. Carleo, L. Tagliacozzo, and L. Sanchez-Palencia, Phys. Rev. B 98, 024302 (2018).
- [32] C. Chen, G. Emperauger, G. Bornet, F. Caleca, B. Gély, M. Bintz, S. Chatterjee, V. Liu, D. Barredo, N. Y. Yao, T. Lahaye, F. Mezzacapo, T. Roscilde, and A. Browaeys, arXiv:2311.11726.
- [33] S. Lepoutre, J. Schachenmayer, L. Gabardos, B. H. Zhu, B. Naylor, E. Maréchal, O. Gorceix, A. M. Rey, L. Vernac, and B. Laburthe-Tolra, Nat. Commun. 10, 1714 (2019).
- [34] A. Patscheider, B. Zhu, L. Chomaz, D. Petter, S. Baier, A.-M. Rey, F. Ferlaino, and M. J. Mark, Phys. Rev. Res. 2, 023050 (2020).
- [35] A. Browaeys and T. Lahaye, Nat. Phys. 16, 132 (2020).
- [36] B. Yan, S. A. Moses, B. Gadway, J. P. Covey, K. R. A. Hazzard, A. M. Rey, D. S. Jin, and J. Ye, Nature (London) 501, 521 (2013).
- [37] A. M. Kaufman and K.-K. Ni, Nat. Phys. 17, 1324 (2021).
- [38] B. Yicheng, Y. Scarlett S., L. Anderegg, C. Eunmi, K. Wolfgang, N. Kang-Kuen, and D. John M., Science 382, 1138 (2023).
- [39] C. M. Holland, Y. Lu, and L. W. Cheuk, Science 382, 1143 (2023).
- [40] L. Chomaz, I. Ferrier-Barbut, F. Ferlaino, B. Laburthe-Tolra, B. L. Lev, and T. Pfau, Rep. Prog. Phys. 86, 026401 (2022).
- [41] L. Su, A. Douglas, M. Szurek, R. Groth, S. F. Ozturk, A. Krahn, A. H. Hébert, G. A. Phelps, S. Ebadi, S. Dickerson, F. Ferlaino, O. Marković, and M. Greiner, Nature (London) 622, 724 (2023).
- [42] T. Legrand, F.-R. Winkelmann, W. Alt, D. Meschede, A. Alberti, and C. A. Weidner, Phys. Rev. A 109, 033304 (2024).
- [43] B. Zhu, A. M. Rey, and J. Schachenmayer, New J. Phys. 21, 082001 (2019).
- [44] See Supplemental Material at http://link.aps.org/ supplemental/10.1103/PhysRevLett.133.203401 for details

- on experimental procedure and simulations, which includes Refs. [45–50].
- [45] V. E. Colussi, H. Kurkjian, M. Van Regemortel, S. Musolino, J. van de Kraats, M. Wouters, and S. J. J. M. F. Kokkelmans, Phys. Rev. A 102, 063314 (2020).
- [46] H. A. M. Leymann, A. Foerster, and J. Wiersig, Phys. Rev. B 89, 085308 (2014).
- [47] D. Plankensteiner, C. Hotter, and H. Ritsch, Quantum 6, 617 (2022).
- [48] A. Polkovnikov, K. Sengupta, A. Silva, and M. Vengalattore, Rev. Mod. Phys. 83, 863 (2011).
- [49] R. Schack and A. Schenzle, Phys. Rev. A 41, 3847 (1990).
- [50] W. Verstraelen, D. Huybrechts, T. Roscilde, and M. Wouters, PRX Quantum 4, 030304 (2023).
- [51] P. J. Lee, B. L. Brown, J. Sebby-Strabley, W. D. Phillips, and J. V. Porto, Nature (London) 448, 452 (2007).
- [52] S. Trotzky, P. Cheinet, S. Fölling, M. Feld, U. Schnorrberger, A. M. Rey, A. Polkovnikov, E. A. Demler, M. D. Lukin, and I. Bloch, Science 319, 295 (2008).
- [53] N. Wurz, C. F. Chan, M. Gall, J. H. Drewes, E. Cocchi, L. A. Miller, D. Pertot, F. Brennecke, and M. Köhl, Phys. Rev. A 97, 051602(R) (2018).
- [54] L. Asteria, H. P. Zahn, M. N. Kosch, K. Sengstock, and C. Weitenberg, Nature (London) 599, 571 (2021).
- [55] K. Mouloudakis and I. K. Kominis, Phys. Rev. A 103, L010401 (2021).
- [56] Y. A. Alaoui, B. Zhu, S. R. Muleady, W. Dubosclard, T. Roscilde, A. M. Rey, B. Laburthe-Tolra, and L. Vernac, Phys. Rev. Lett. 129, 023401 (2022).
- [57] G. W. Oehlert, Am. Stat. 46, 27 (1992).
- [58] Y. A. Alaoui, Studies of spin correlations in an ensemble of lattice trapped dipolar atoms, Ph.D. thesis, Université Sorbonne Paris Nord, 2022.
- [59] N. Gemelke, X. Zhang, C.-L. Hung, and C. Chin, Nature (London) **460**, 995 (2009).
- [60] A. L. Kuzemsky, J. Low Temp. Phys. 206, 281 (2022).
- [61] S. Braun, J. P. Ronzheimer, M. Schreiber, S. S. Hodgman, T. Rom, I. Bloch, and U. Schneider, Science 339, 52 (2013).
- [62] K. Honda, S. Taie, Y. Takasu, N. Nishizawa, M. Nakagawa, and Y. Takahashi, Phys. Rev. Lett. 130, 063001 (2023).
- [63] J. Schachenmayer, A. Pikovski, and A. M. Rey, Phys. Rev. X 5, 011022 (2015).
- [64] S. R. Muleady, M. Yang, S. R. White, and A. M. Rey, Phys. Rev. Lett. 131, 150401 (2023).
- [65] J. Wurtz, A. Polkovnikov, and D. Sels, Ann. Phys. (Amsterdam) **395**, 341 (2018).
- [66] V. Giovannetti, S. Mancini, D. Vitali, and P. Tombesi, Phys. Rev. A 67, 022320 (2003).
- [67] S. Sugimoto, R. Hamazaki, and M. Ueda, Phys. Rev. Lett. 129, 030602 (2022).
- [68] Y. Levin, R. Pakter, F. B. Rizzato, T. N. Teles, and F. P. Benetti, Phys. Rep. 535, 1 (2014).